Available online at www.sciencedirect.com
SCIENCE DIRECT®
International Journal of Heat and Fluid Flow 25 (2004) 933–944
International Journal of HEAT AND FLUID FLOW
www.elsevier.com/locate/ijhff

An investigation of the heat transfer and static pressure on the over-tip casing wall of an axial turbine operating at engine representative flow conditions. (I). Time-mean results

S.J. Thorpe [a,*], S. Yoshino [b,1], R.W. Ainsworth [a], N.W. Harvey [c]

[a] Department of Engineering Science, University of Oxford, Parks Road, Oxford, OX1 3PJ, UK
[b] Tokyo Electric Power Company, Thermal Power Technology Group, 4-1 Egasaki-cho, Tsurumi-ku, Yokohama, 230-8510, Japan
[c] Rolls-Royce plc, Turbine Systems (PCF-2), PO Box 31, Derby, DE23 6AY, UK

Received 17 November 2003; accepted 20 February 2004
Available online 20 May 2004

Abstract

The over-tip casing of the high-pressure turbine in a modern gas turbine engine is subjected to strong convective heat transfer that can lead to thermally induced failure (burnout) of this component. However, the complicated flow physics in this region is dominated by the close proximity of the moving turbine blades, which gives rise to significant temporal variations at the blade-passing frequency. The understanding of the physical processes that control the casing metal temperature is still limited and this fact has significant implications for the turbine design strategy. A series of experiments has been performed that seeks to address some of these important issues. This article reports the measurements of time-mean heat transfer and time-mean static pressure that have been made on the over-tip casing of a transonic axial-flow turbine operating at flow conditions that are representative of those found in modern gas turbine engines. Time-resolved measurements of these flow variables (that reveal the details of the blade-tip/casing interaction physics) are presented in a companion paper. The nozzle guide vane exit flow conditions in these experiments were a Mach number of 0.93 and a Reynolds number of 2.7×10^6 based on nozzle guide vane mid-height axial chord. The axial and circumferential distributions of heat transfer rate, adiabatic wall temperature, Nusselt number and static pressure are presented. The data reveal large axial variations in the wall heat flux and adiabatic wall temperature that are shown to be primarily associated with the reduction in flow stagnation temperature through the blade row. The heat flux falls by a factor of 6 (from 120 to 20 kW/m^2). In contrast, the Nusselt number falls by just 36% between the rotor inlet plane and 80% rotor axial chord; additionally, this drop is near to linear from 20% to 80% rotor axial chord. The circumferential variations in heat transfer rate are small, implying that the nozzle guide vanes do not produce a strong variation in casing boundary layer properties in the region measured. The casing static pressure measurements follow trends that can be expected from the blade loading distribution, with maximum values immediately upstream of the rotor inlet plane, and then a decreasing trend with axial position as the flow is turned and accelerated in the relative frame of reference. The time-mean static pressure measurements on the casing wall also reveal distinct circumferential variations that are small in comparison to the large pressure gradient in the axial direction.

Keywords: Heat transfer; Turbine; Tip leakage; Aerothermodynamics; Transonic; Thin-film gauge

1. Introduction

The tip-clearance region of a high-pressure axial-flow turbine provides a significant design challenge for gas turbine engine manufacturers. Important factors such as overall turbine efficiency, heat loading, cooling airflow requirements and component durability are all influenced by the complex flow phenomena occurring in this severe environment. However, the published experimental data for both blade-tip and over-tip casing heat transfer is extremely limited for engine representative flow conditions, and it would appear that manufacturers continue to rely on expensive engine experience rather than an appropriate aero-thermal design methodology based on detailed physical understanding (Bunker,

* Corresponding author. Tel.: +44-1865-288735; fax: +44-1865-288756.
E-mail address: steve.thorpe@eng.ox.ac.uk (S.J. Thorpe).
[1] Current address: Tokyo Electric Power Company, Tokyo, Japan.

0142-727X/$ - see front matter © 2004 Elsevier Inc. All rights reserved.
doi:10.1016/j.ijheatfluidflow.2004.02.027

Nomenclature

c	specific heat capacity	T	temperature
C_{ax}	axial chord length	V_g	heat transfer gauge voltage
h	heat transfer coefficient		
i_g	heat transfer gauge current	*Greeks*	
k	thermal conductivity	ρ	density
Nu	Nusselt number		
$\dot{Q}$	heat transfer rate	*Subscripts*	
R	heat transfer gauge resistance	aw	adiabatic wall
t	time	w	wall

2001). An additional complexity for the design of the over-tip casing wall is that the aerodynamic and heat transfer processes are strongly influenced by the close proximity of the moving turbine blades; this fact gives rise to periodic disruption of the casing boundary layer, and therefore large temporal variations in heat transfer at the blade passing frequency (Guenette et al., 1985). The specific details of these temporal variations depend upon the particular flow physics present in the tip-gap, with the gap-height and blade pressure distribution being primary factors in this respect. Indeed, this is an area that is currently poorly understood for the engine situation. In modern gas turbine engines, the drive toward ever higher thermal efficiency has increased combustor exit temperatures to levels that require the high-pressure turbine to operate in a temperature environment that could severely compromise its structural integrity or, in the worst case, lead to component burnout. Consequently, the understanding of heat transfer phenomena is a significant contributor to engine reliability and the commercial competitiveness of engine suppliers. To mitigate against thermally induced turbine failure, engine manufacturers employ a combination of thermal barrier coatings (see for example, Meetham, 1984) and combustor by-pass cooling air (see for example, Dailey, 2000) with the aim of maintaining metal temperatures below appropriate limits. Significantly, the use of cooling air detracts from the overall thermal efficiency of the engine and, as a consequence, manufacturers continue to seek improvements in their designs that minimise such penalties. It is evident that an efficient design process for the over-tip casing requires a knowledge of the heat load imposed on it at a particular turbine running condition. The availability of this knowledge will allow the appropriate wall cooling configuration to be arrived at in a more timely fashion and at reduced overall product development cost.

It is from this background that a significant body of published work has accumulated over several decades on the basic over-tip leakage flow physics in unshrouded axial turbines. However, the significant experimental difficulties associated with obtaining measurements that are representative of (and scaleable to) the engine case have meant that the bulk of this work has concentrated on low-speed analogies of the tip-clearance flow, rather than being appropriately scaled using all applicable non-dimensional parameters. In these studies then, typically the Reynolds number is matched to the engine case but Mach number and relative motion between casing and blade are not reproduced. Additionally, most work in this area has concentrated on measurements related to the blade-tips rather than over-tip casing. However, these qualitative investigations have provided considerable insight into the fundamental mechanism by which the blade loading distribution produces a pressure difference that drives the over-tip leakage flow, and have shown the way in which this forms into a tip-leakage vortex in the suction surface/casing endwall corner (Yamamoto, 1988; Bindon, 1988). Detailed measurements of the development of this vortex, and its interaction with the passage flow, have enabled the estimation of aerodynamic losses associated with the tip-clearance flow (Kaiser and Bindon, 1997). The effect of blade-tip treatments and tip-gap height on the tip-leakage aerodynamics have also been investigated in the context of low-speed experiments on large blade models (Heyes et al., 1992). Heat transfer measurements in the over-tip region of axial turbines are more limited in scope than the aerodynamic investigations. Some measurements of blade-tip heat transfer in low-speed rigs have been obtained, for example, the work of Kim and Metzger (1995), Papa et al. (2003) and Srinivasan and Goldstein, 2003. These experiments have been important for the development of a qualitative understanding of the flow physics, and for investigating the influence of factors such as tip-gap height, tip geometry and blade/casing relative motion. However, the direct relevance of these low-speed tests to the engine flow conditions does not appear to have been quantified. Since the actual flow through a high-pressure turbine tip-gap is compressible, shock waves and shock/boundary layer interaction are of significance to both the aerodynamics and heat transfer phenomena (Moore et al., 1988). Indeed, the published literature contains only a small quantity of

heat transfer data that has been gathered at the correct non-dimensional flow conditions for the over-tip casing. For example, Guenette et al. (1985) report the measurement of time-resolved over-tip casing heat transfer and static pressure, although the measurements were restricted to one axial row of measurement locations (that is, at a fixed pitch relative to the nozzle guide vane locations). These workers measured the unsteady heat transfer at seven axial positions through the rotor tip-gap, and were able to identify clearly the strong influence of the blade passing on the unsteady casing heat transfer rate. Mean heat transfer rates were seen to decrease rapidly with axial distance through the turbine rotor, the cause of this being identified as the falling stagnation temperature as well as variations in heat transfer coefficient. The work of Guenette included the measurement of the effect of Reynolds number and turbine specific speed. However, the investigations by Guenette et al. (1985) did not include the measurement of the local adiabatic wall temperature distribution through the rotor and consequently did not report an appropriately defined Nusselt number (hence the results cannot be scaled to the engine case). Metzger et al. (1991) have also reported the measurement of heat flux to the casing wall of a turbine operating at flow conditions representative of those found in modern gas turbines. The heat flux was seen to fall with increasing axial distance along the over-tip casing wall. Unfortunately, these workers also failed to report the spatial variation in adiabatic wall temperature and were similarly unable to report a true non-dimensional heat transfer rate. Unsteady static pressure measurements on the casing wall of a turbine operating at appropriate Mach and Reynolds numbers have been reported by Kingcombe et al. (1990). In this work a single row of measurement locations was used; these being arranged along an approximate flow streamline. These data showed that the magnitude of the pressure fluctuation on the casing wall was in agreement with that expected by consideration of the blade loading distribution.

In addition to over-tip casing measurements, several investigations of nozzle guide vane endwall heat transfer have been made at engine representative flow conditions. This work is significant in the context of the current investigation as it provides insight into the likely heat transfer conditions immediately upstream of the moving blade row. For example, Spencer et al. (1996) report casing endwall heat transfer coefficient measurements through a transonic nozzle guide vane at a range of Mach and Reynolds numbers.

The principle aims of the experimental programme reported here have been the measurement of the time-mean and time-varying heat flux, adiabatic wall temperature, Nusselt number and static pressure on the stationary over-tip casing of an axial turbine operating at flow conditions that are representative of those found in modern gas turbine engines. In particular, the correct non-dimensional scaling of the turbine requires the employment of appropriate Mach and Reynolds numbers, gas to wall temperature ratio and turbine specific speed in the experiments. The complexities of this high-speed experiment are significant and challenging when compared to low-speed investigations of tip leakage. However, the correct experimental modelling of the flow physics is essential to further the understanding of turbine tip leakage, and this work complements the large amount of data that has been accumulated in low-speed testing over the last two decades. In real gas turbine engines the tip leakage involves transonic flow regimes and some regions of the tip-leakage flow may be supersonic in both stationary and blade-relative frames of reference (as first suggested by Moore et al. (1988)). Consequently, shock waves will be present within the tip-gap and these will track around the annulus with the blade-tips. These compressible flow features will have a significant impact on both the aerodynamics and heat transfer; such effects are clearly absent from low-speed testing. In addition, it is important to model the thermodynamics of the turbine: large work processes establish temporal and spatial variations in the flow total temperature through the turbine stage. It is worth noting here an important difference between the experimental modelling requirements for the blade-tip and those for the stationary over-tip casing: in the blade-relative frame of reference the flow over the blade-tips is comparatively steady (except for the influence of the upstream vanes), while the flow at a point on the outer casing wall is massively unsteady due to the close proximity of the moving blades. As a result, a primary characteristic of the flow on the casing is the unsteadiness generated by the moving blades (at a frequency of tens of kHz), which cause rapid periodic fluctuation in flow direction, speed, pressure and temperature. Importantly, the experiments presented here incorporate the full impact of these unsteady flow features on the casing aerodynamics and heat transfer.

The data produced in this work is divided into sections that cover time-mean and time-resolved data; these are presented in this paper and a companion paper, respectively (Thorpe et al., 2004). These data provide fundamental information on the casing heat load and the aerodynamic interaction between stationary casing and moving blades; through this it has consequently been possible to expand the understanding of the tip-gap flow physics.

2. Experimental approach

The measurements described in this paper have been performed on the short duration transonic axial-flow turbine facility located at the Department of Engineering

Science in the University of Oxford. This Isentropic Light Piston Tunnel facility has been described in detail in several previous publications (for example, Ainsworth et al., 1988; Ainsworth et al., 1989), and only a brief summary of the test apparatus will be provided here. Previously, this test facility has been used to measure the unsteady pressure and unsteady heat transfer on rotating blades, and more recently the interaction between high-pressure turbine and intermediate-pressure guide vanes (Dietz and Ainsworth, 1992; Garside et al., 1994; Miller et al., 2003). A schematic diagram of the experimental apparatus is presented in Fig. 1. The wind tunnel consists of three primary components: (i) a large tube in which is mounted a freely moving piston; (ii) the working section where the stator and rotor are mounted and (iii) a large evacuated dump tank. The turbine stage consists of 36 nozzle guide vanes having an axial chord of 30 mm, and 60 rotor blades having an axial chord of 24 mm. The stage inlet stagnation conditions are a pressure of 8.04 bar and a temperature of 374 K. The conditions at nozzle guide vane exit are a Mach number of 0.93 and a Reynolds number of 2.7×10^6 (conditions at mid-height and based on vane axial chord). The turbulence intensity of the inlet flow is 2.5%. The turbine operating parameters are summarised in Table 1. The rotor tip-clearance for this facility is 1.2 mm or 2.5% of span, measured under static (non-rotating) conditions. This tip-gap is representative of that found in an engine where oxidation and erosion of the blade-tips has occurred i.e. an engine that has been in service for some time. This is larger than the gap to be expected in the high-pressure turbine of a "new" gas turbine engine, which would normally be in the region of 1% of blade span. However, as will be seen in Part II of this work, the emphasis is on generating an understanding of the general flow physics of the tip-gap region.

The operation of the turbine facility can be summarised briefly as follows. Prior to the start of a test the piston is positioned at the furthest most point from the working section, and an annular gate valve seals the

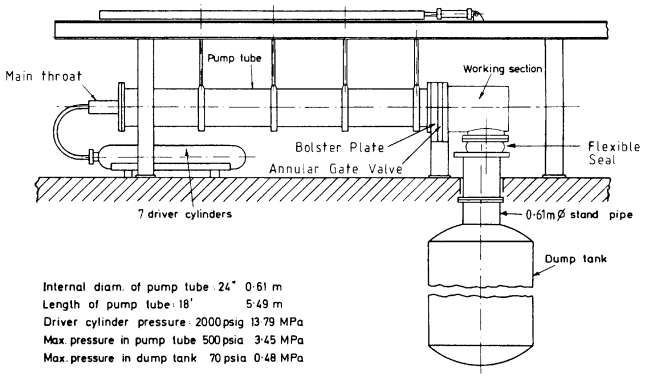

Fig. 1. A schematic diagram showing the main components of the Oxford University transonic turbine test facility.

Table 1
A summary of the turbine operating parameters in the Oxford Rotor Facility

Parameter	Value	Units
Inlet total pressure	8.04	bar
Inlet total temperature	374	K
NGV exit Mach number	0.93	–
Specific speed	436	rpm/$K^{1/2}$
Mass flow number	7.0×10^{-4}	ms $K^{1/2}$
Reynolds number (based on NGV exit flow, and NGV axial chord)	2.7×10^6	–
Tip-clearance (static)	1.2	mm
Rotor tip diameter	0.55	m
Rotational speed	8910	rpm
Total run-time	200	ms
Vane–blade axial gap	11	mm
NGV exit flow angle	70	degrees
Rotor relative inlet flow angle	35	degrees
Rotor relative exit flow angle	−63	degrees

piston tube from the working section and dump tank, which are initially evacuated. The rotor is accelerated by an air motor to a predetermined speed (7150 rpm) at which point high-pressure air is introduced rapidly behind the piston through a set of sequenced valves, thereby forcing the piston to start moving toward the gate valve and to compress the gas in front of it. When the pressure in front of the piston reaches the appropriate level, the fast acting gate valve opens, allowing the isentropically compressed air to pass through the turbine and in to the evacuated dump tank. The work produced by the rotor causes its rotational speed to increase, and during this acceleration the speed passes through the design value (8910 rpm). The piston tube generates a short duration air flow that is at elevated pressure and temperature and establishes aerodynamic conditions within the turbine that are representative of those found in a modern high-pressure turbine but without using the high gas temperatures found in real engines; a summary is presented in Table 1.

The turbine test facility is extensively instrumented with sidewall pressure tappings, total pressure probes, thermocouples and shaft speed encoders. These signals are recorded by a 64 channel transient data capture system that digitises the signals at typically 5 kHz. These data enable the tunnel operating conditions to be monitored at various axial locations. A second high-speed transient capture system is employed to record wide-bandwidth signals from instrumentation such as Kulite piezo-resistive pressure transducers, heat transfer gauges, hot-wire anemometers and optical encoders. Again, 64 channels of this fast data recording are available with sampling rates typically between 200 and 500 kHz at 12-bit resolution. The data accumulated during a test is downloaded to a personal computer with which signal processing is conducted. This allows rapid output of processed data (turbine operating parameters)

that enable the operator to verify the run conditions and instrumentation function.

3. Casing wall instrumentation

3.1. The measurement of heat transfer rate

The Isentropic Light Piston Tunnel facility is particularly suited to the investigation of heat transfer phenomena, primarily because an appropriate gas to wall temperature ratio can be maintained throughout the duration of the experiment (Ainsworth et al., 1989). Traditionally, this approach to the measurement of heat transfer has relied upon the use of thin-film resistance thermometers to determine the surface temperature history on the wall of an experimental model (Schultz and Jones, 1973). Under the assumptions of one-dimensional heat conduction into the solid wall and semi-infinite substrate thickness, these data enable the time-dependent surface heat transfer rate to be determined. Typical bandwidths for this type of instrumentation can be in excess of 100 kHz and are therefore appropriate to the measurement of unsteady heat fluxes in turbine environments where blade passing frequencies are typically in the region of 10 kHz (in the Oxford rotor the blade passing frequency is 8.9 kHz).

A primary goal for this work was the measurement of both temporal and spatial variations in heat transfer rate on the casing wall. This requirement established two additional constraints on the fabrication of the instrumentation. Firstly, the physical size of the temperature measuring element would need to be reduced compared to previous studies, thereby allowing finer spatial resolution in the measurement system, and higher packing density of measurement points (gauges) on the casing wall. Secondly, the positioning of the individual gauges would need to be accurately controlled in an array of defined measurement locations. In response to these demands, a novel fabrication strategy was devised that employs a pulse laser to cut gauge and electrically conducting track patterns in a test model surface that has been metallised with a thin-film of platinum. This technique has proven extremely useful in the repeatable manufacture of heat transfer gauges that are typically 1.2×0.08 mm in size (Thorpe et al., 2000).

The instrumented section of the casing wall was manufactured from Macor machineable glass ceramic and mounted in the over-tip casing ring on the turbine test facility. The instrumented surface of the Macor was polished using various diamond based abrasives to produce a mirror-like finish suitable for the deposition of metallic thin-films. Standard organo-metallic platinum ink (Engelhard 05X) was used to metallise the polished surface and laser cutting of the gauge and track pattern was employed (Thorpe et al., 2000). A schematic

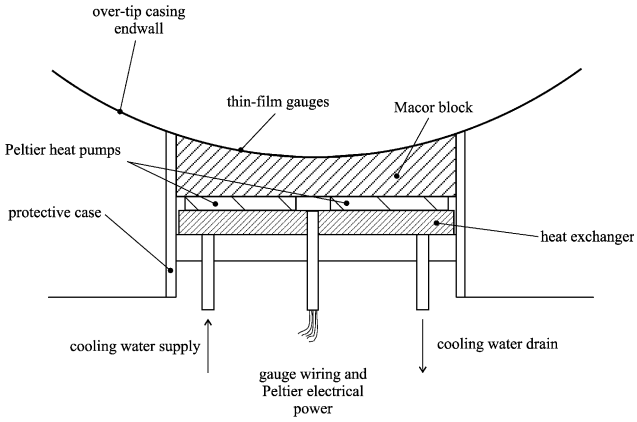

Fig. 2. A schematic diagram that shows a cross-sectional view of the instrumented over-tip casing wall sector.

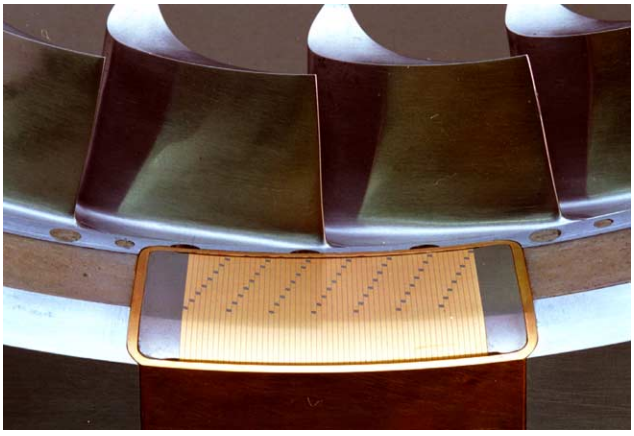

Fig. 3. A photograph of the over-tip casing heat transfer instrumentation.

diagram of the instrumented casing sector is shown in Fig. 2 and a photograph is shown in Fig. 3.

The measurement locations used in this study are defined in the schematic diagram shown in Fig. 4. The gauge positions form a regular array of seven positions in the circumferential direction on a 1 mm pitch and eight positions in the axial direction, making a total of 56 measurement locations. The circumferential extent of the array is 1 nozzle guide vane pitch, while the axial extent is from −20% to +80% rotor axial chord. This arrangement gives two circumferential lines of gauges upstream of the blade row inlet plane (an important measurement that determines the heat transfer rate associated with NGV exit conditions in a region largely undisturbed by blade passing). As denoted in Fig. 4, the circumferential positions are identified by letters A–G, while the axial positions are denoted by numbers 1–8. This nomenclature is used throughout this article when referring to particular gauge positions.

Consideration of the signal to noise ratio in the heat transfer measurements, and Ohmic self-heating of the

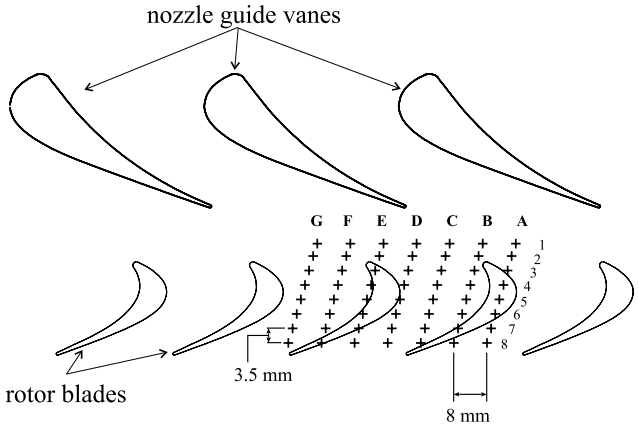

Fig. 4. A diagram that illustrates the location of heat transfer and static pressure measurement positions on the over-tip casing wall.

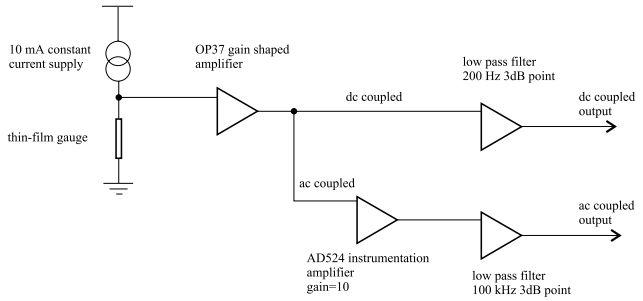

Fig. 5. A schematic diagram of the heat transfer gauge amplifier and signal conditioning electronics.

miniature gauges has indicated that the electrical resistance of the platinum thin-film gauges should be in the range 75–150 Ω. The variation of electrical resistance with temperature was calibrated for each gauge in the range 20–60 °C using a temperature controlled stirred water bath into which the entire instrumented block was placed. The calibration technique involved measuring the gauge resistance as a function of temperature over a cycle of increasing and decreasing temperatures. Indeed this is the primary quality control test on the electrical performance of the heat transfer gauges, and reveals any hysteresis in the resistance/temperature response; appropriate annealing cycles can be employed if required. The temperature coefficient of resistance was in the range 0.00260–0.00275 for all gauges.

Custom-built heat transfer gauge excitation and amplifier units were developed specifically for this measurement campaign, and a schematic diagram of the circuit is presented in Fig. 5. The overall design of the electronics allows the accurate measurement of high frequency heat transfer signals (through the ac output coupling) whilst also enabling the measurement of the absolute gauge temperature (dc output coupling). The platinum resistance gauges were excited with a nominal 10 mA constant current that was measured for each gauge immediately prior to a Rotor Facility test. The gauge voltage was amplified with a frequency dependent amplifier (similar to that used by Ainsworth et al., 1989) that has a gain profile that increases from 5 at dc to 500 at 100 kHz. The amplified signal was then coupled to ac and dc mode outputs. In addition, the ac coupled signal could be amplified by an AD524 (manufactured by Analog Devices) instrumentation amplifier with a flat frequency response and gain of 10. The frequency response of all heat transfer gauge amplifier units was calibrated in the frequency range 0–200 kHz, with this information being used in signal processing algorithms.

3.2. The measurement of adiabatic wall temperature

A significant goal for the experimental programme reported here was the measurement of the spatial distribution of Nusselt number on the casing wall. For this to be achieved, it was essential that the instrumentation and experimental technique allowed the measurement of local adiabatic wall temperature at each heat transfer gauge location. This is particularly important for the flow in the region of the over-tip casing since the gas total temperature falls considerably through the rotor as work is extracted by the turbine (the total temperature falls from 374 to 290 K between the inlet and exit planes). Clearly then, the adiabatic wall temperature will be a strong function of position in these casing wall measurements. A novel technique was devised at an early stage in the development of the instrumentation that would allow the determination of adiabatic wall temperature in the short duration turbine facility. This will be described in the remainder of this section.

In the experiments reported here the determination of adiabatic wall temperature relies upon the measurement of the time-mean heat transfer rate at a range of casing wall temperatures. The data produced in this way can be plotted as shown in Fig. 6. This figure shows the variation in heat transfer rate as a function of wall temperature for a typical heat transfer gauge. The straight line that fits the experimental data in a least squares sense is shown in Fig. 6. From the straight line fit both the mean heat transfer coefficient and adiabatic wall temperature can be extracted. By inspection of Eq. (1), it can be seen that the adiabatic wall temperature is found from the point where the heat transfer rate is zero, while the heat transfer coefficient is established from the gradient of the straight line fit.

$$\dot{Q} = h(T_{\mathrm{aw}} - T_{\mathrm{w}}) \tag{1}$$

In order to make adiabatic wall temperature measurements, the instrumented casing wall sector shown in Fig. 2 includes the capability to vary the instrumented Macor

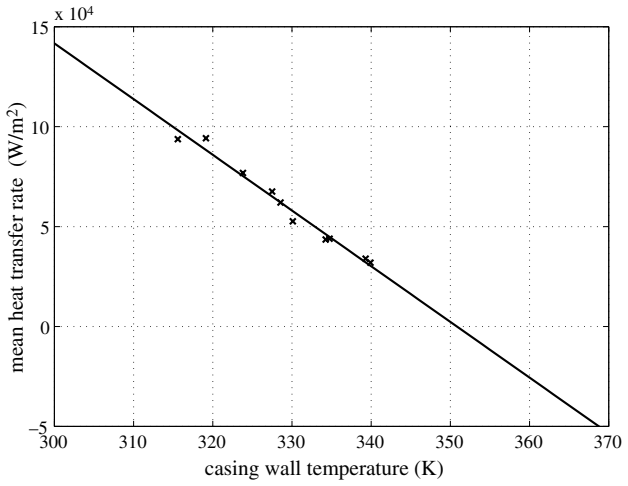

Fig. 6. A graph that illustrates the variation in measured time-mean heat transfer rate as a function of casing wall temperature.

block temperature prior to a test in the rotor facility. This is achieved using two Peltier heat pump devices that are embedded in the base of the Macor block (Fig. 2). This allows the block to be either heated or cooled prior to a test in the Rotor Facility. The level of heating or cooling can be varied by adjustment of the excitation voltage, and in this way different wall temperatures can be established before a test. The Peltier heat pumps are sandwiched between the Macor block and a copper heat exchanger. This heat exchanger can be cooled using circulating water and allows heat to be absorbed from the heat pumps. On a succession of Rotor Facility experiments, the wall temperature can therefore be set to different values and the corresponding variation in mean heat transfer rate to the casing wall can be measured (as shown in Fig. 6). Typically, 10 different wall temperatures have been employed in this procedure, covering a temperature range of between 15 and 30 K depending upon the gauge position. This type of data has been measured for all heat transfer gauges on the casing wall, and therefore the spatial distribution of adiabatic wall temperature established.

3.3. The measurement of static pressure

In order to promote the full understanding of the heat transfer data, the static pressure distribution on the casing wall has been measured at an equivalent set of locations on the casing wall. To achieve this a second instrumented wall sector was manufactured that incorporates 56 static pressure tappings at exactly the same locations as the heat transfer gauges. These tappings are 1 mm in diameter and 0.5 mm deep. The bandwidth of the Kulite sensors mounted in this configuration is in excess of 100 kHz.

4. Experimental results

The extensive database of heat transfer and pressure measurements obtained in this study can be grouped into two distinct categories: (1) time-mean values; (2) time-varying values. In each of these groups the data are further divided into heat transfer rate, adiabatic wall temperature, Nusselt number and static pressure. This paper reports the time-mean measurements, whilst the companion paper (Thorpe et al., 2004) reports the time-resolved data. A detailed description of the time-mean results will be given in the following sections. Note that an assessment of the measurement uncertainties is presented in Appendix A.

4.1. Time-mean heat transfer rate

The measured time-mean heat transfer rate distribution on the casing wall is presented in Fig. 7a and b for the 56 heat transfer gauge positions. The heat transfer rate is highest in the two circumferential rows of measurement positions that are upstream of the rotor leading edge (approximately 140 kW/m^2). In the blade over-tip region (gauge rows 3–8) the casing heat transfer rate drops gradually to 100 kW/m^2 at 35% rotor axial chord, followed by a more rapid decrease with axial distance beyond this point. At 80% rotor axial chord (gauge row 8), the time-mean heat transfer rate to the casing is approximately 20 kW/m^2 or less than one fifth of that at the rotor inlet plane. These trends are in qualitative agreement with expectation and primarily reflect the decrease in total temperature of the working fluid as energy is extracted by the rotor. Hence this drop in heat transfer is closely related to the blade loading distribution and thereby the distribution of work production through the machine. The primary effect of this is the reduction in the heat transfer driver temperature ($T_{aw} - T_w$), and therefore the heat transfer rate as will be shown in the next section. Of course, there will also be a variation in heat transfer rate caused by changes in heat transfer coefficient through the rotor, and these will also be considered in due course.

The circumferential variation in heat transfer rate at a particular axial station is seen in Fig. 7a and b to be relatively small, with variations no greater than ±10% at all axial locations. A region of highest heat transfer rate that is associated with the nozzle guide vane trailing edge is evident in the data shown in Fig. 7a, although this is a small effect compared to the other factors that influence the spatial variations. The physical cause of the high heat transfer in this region will be shown to be a vane–blade interaction (Thorpe et al., 2004).

Very little comparable data exists in the open literature. However, Metzger et al. (1991) have reported a limited data-set of casing wall measurements in a turbine operating at engine representative flow conditions.

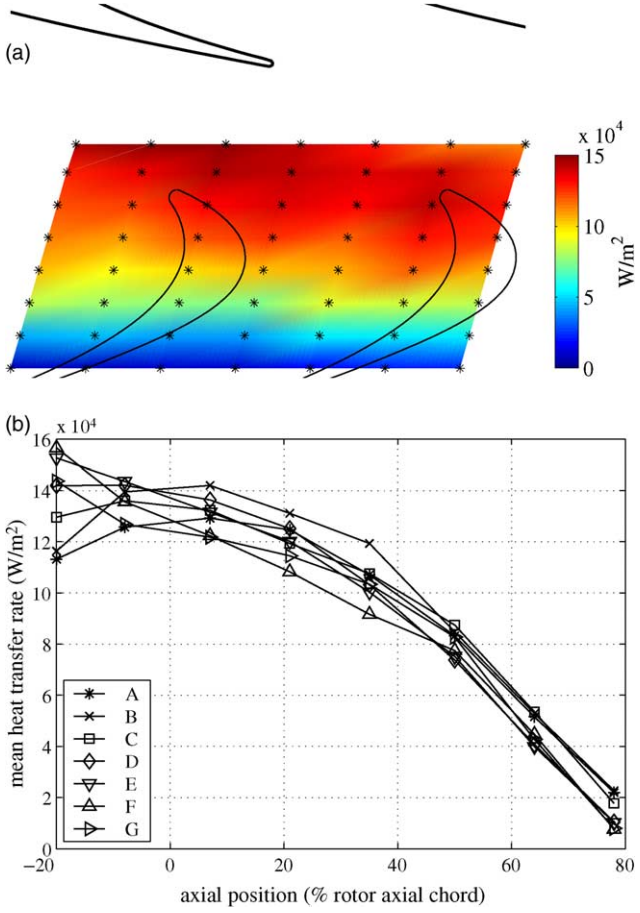

Fig. 7. (a) A colour contour plot showing the measured time-mean heat transfer rate distribution on the casing wall (* symbols indicate heat transfer gauge locations), (b) a graph showing the measured time-mean heat transfer rate to the over-tip casing wall (letters A–G refer to heat transfer gauge definitions given in Fig. 4).

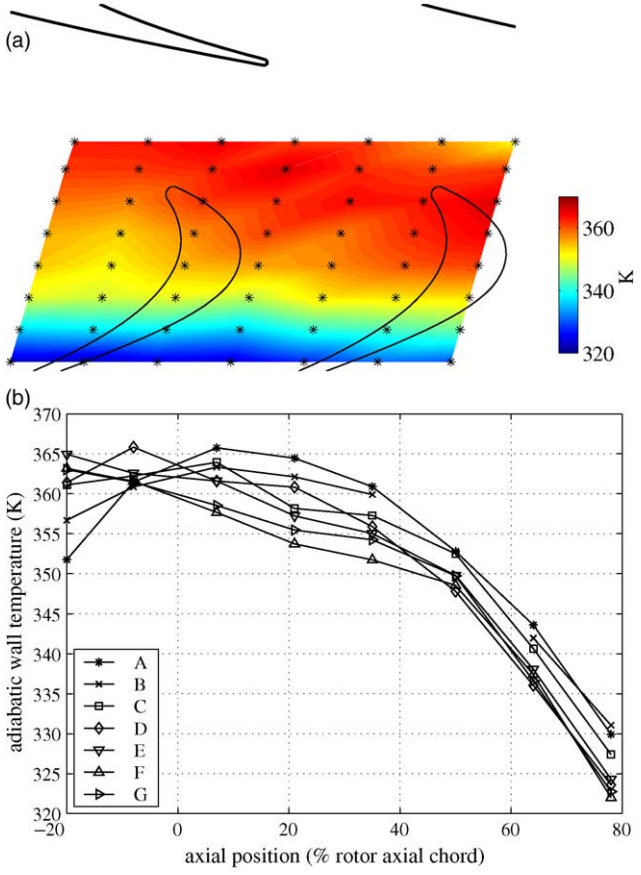

Fig. 8. (a) A colour contour plot showing the measured time-mean adiabatic wall temperature distribution on the casing wall (* symbols indicate heat transfer gauge locations), (b) a graph showing the measured time-mean adiabatic wall temperature on the over-tip casing wall (letters A–G refer to heat transfer gauge definitions given in Fig. 4).

In their measurements, which were conducted at a range of tip-clearances, Metzger et al. observed a falling trend in heat flux through the turbine rotor in a roughly linear manner. In the work of Guenette et al. (1985), the variation of time-mean casing heat flux is presented as a function of axial position at a variety of flow Reynolds numbers and turbine speeds for a limited number of measurement points. Very similar trends in the heat transfer data were observed at the design aerodynamic conditions. Note that in both of these previous experimental studies the measurement of local adiabatic wall temperature was not reported, and that as a consequence the true Nusselt number was not determined.

4.2. Time-mean adiabatic wall temperature

The measured time-mean adiabatic wall temperature distribution is shown in Fig. 8a and b for the 56 measurement locations on the casing wall. The data show that the flow recovery temperature is highest upstream of the rotor leading edge (360–365 K) in the gap between NGV exit and rotor inlet planes.

Reflecting similar trends to the mean heat transfer rate data, the adiabatic wall temperature decreases slightly from the rotor leading edge to 35% rotor axial chord and then falls more quickly beyond this point toward the trailing edge. The adiabatic wall temperature on the casing at 80% rotor axial chord is in the range 322–330 K, depending upon circumferential position. The overall decrease in adiabatic wall temperature through the rotor is indicative of the fall in absolute total temperature through the turbine as work is extracted from the flow and the angular velocity of the fluid is reduced. The circumferential variations in adiabatic wall temperature are small compared to the large variations that occur in the axial direction. However, the small circumferential effects that are evident are related to the interaction between blade and vane, and in particular the periodic changes in lift that occur as the blades move around the annulus: this will be explored in Part II of this work.

The time-mean adiabatic wall temperature upstream of the rotor can be estimated from the known flow conditions at NGV exit and the temperature recovery factor associated with the turbulent boundary layer at NGV exit conditions (Mach number 0.85). Assuming a temperature recovery factor of 0.86 (Schlichting and Gersten, 2000), the predicted recovery temperature is 367 K which is in close agreement with the measured values.

The adiabatic wall temperature is related to the flow total temperature by a recovery factor that is Mach number dependent. Consequently the adiabatic wall temperature can be interpreted as a local total temperature as long as the Mach number is known. Even if the Mach number is not known exactly, the difference between these two temperatures is less than 8 K for a Mach number of 0.9 and total temperature of 374 K. At a qualitative level at least, the data presented in Fig. 8a can be considered to represent a "slice" of time-mean thermodynamic data, namely the absolute total temperature adjacent to the casing wall. By considering the data in this way, the distribution of recovery temperature also signifies where work is being produced by the fluid: a low temperature indicates that the fluid has produced work, a high temperature that it has not. This concept is explored more in Part II of this work, where the measured unsteady recovery temperature is used to explore the work processes that occur within the blade row.

4.3. Time-mean Nusselt number

The measurement of heat transfer rate and adiabatic wall temperature for each gauge permits the calculation of mean Nusselt number by application of Eq. (2).

$$Nu = \frac{\dot{Q}}{T_{aw} - T_w} \frac{C_{ax}}{k} \tag{2}$$

where the length scale is taken as the rotor axial chord, and the thermal conductivity of the gas is evaluated at the local, experimentally measured flow recovery temperature. The measured time-mean Nusselt number distribution on the casing wall is presented in Fig. 9a

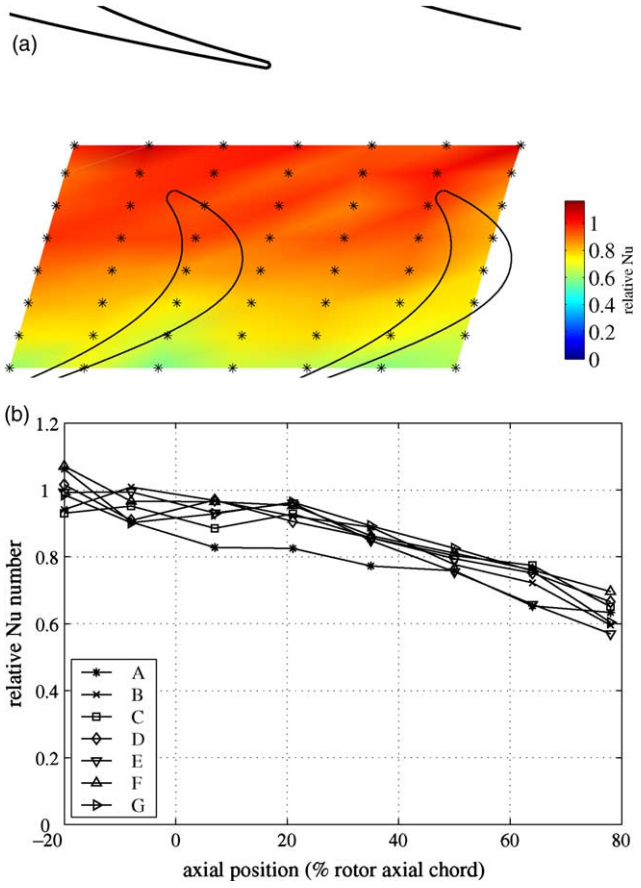

Fig. 9. (a) A colour contour plot showing the measured time-mean Nusselt number distribution on the casing wall (* symbols indicate heat transfer gauge locations), (b) a graph showing the measured time-mean Nusselt number on the over-tip casing wall (data normalised to the circumferentially averaged value at −20% rotor axial chord; letters A to G refer to heat transfer gauge definitions given in Fig. 4).

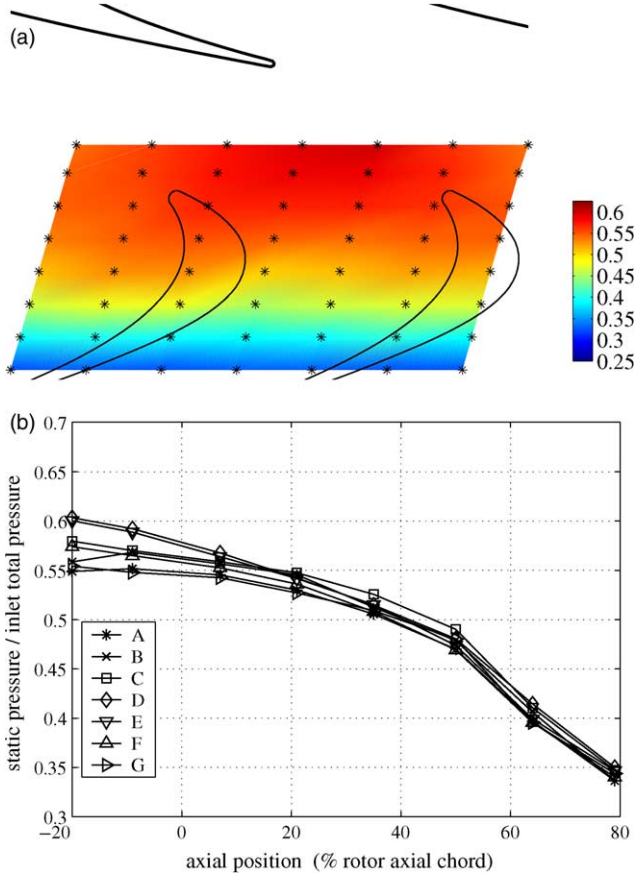

Fig. 10. (a) A colour contour plot showing the measured time-mean static pressure distribution on the casing wall (normalised by the stage inlet total pressure; * symbols indicate pressure gauge locations), (b) a graph showing the measured time-mean static pressure on the over-tip casing wall (letters A–G refer to pressure gauge definitions given in Fig. 4).

and b (note that this data is normalised by the mean value at −20% rotor axial chord). The Nusselt number is highest in the gap between guide vane exit and rotor inlet planes, with a relatively slow decrease up to 21% rotor axial chord. Beyond this point there is a near linear decrease in Nusselt number with increasing axial distance through the rotor. In fact, the value reduces by 36% between rotor inlet plane and 80% axial chord.

The data reveal that there are only minor variations in time-mean Nusselt number associated with circumferential position, implying that the influence of the nozzle guide vane exit flow features is small. Interestingly, while there are strong axial variations in mean heat transfer rate (Fig. 7a), these are primarily associated with variations in adiabatic wall temperature (Fig. 8a) rather than the Nusselt number. This demonstrates the importance of measuring the local adiabatic wall temperature on the turbine casing.

The authors consider that there are two primary physical factors that control the distribution of the time-mean Nusselt number on the casing wall. Firstly, the variation of the flow time-mean Reynolds number, which decreases through the turbine as the flow is decelerated and expanded. Consideration of the effect of Reynolds number on the heat transfer in a turbulent boundary layer suggests that the casing Nusselt number will fall through the rotor. Secondly, the flow conditions next to the casing wall are disturbed periodically by the moving turbine blades (at a frequency of 8.9 kHz), leading to a disruption of the casing boundary layer state, and a subsequent increase in heat transfer. This aspect of the flow physics will be considered in more detail in Part II of this work (Thorpe et al., 2004).

4.4. Time-mean static pressure

The measured time-mean static pressure distribution on the casing wall is presented in Fig. 10a and b. The data reveal the generally expected variation of static pressure through the turbine stage with highest pressures associated with the gap between guide vanes and blades, and with falling pressure thereafter as the flow is accelerated in the rotor relative frame of reference. Static pressure decreases slowly from rotor inlet to 50% axial chord, with a more rapid decrease after this (a trend that was also seen in heat transfer rate and adiabatic wall temperature). There are small but distinct circumferential variations in static pressure in the inter-row gap, with static pressure being highest in locations D1 and E1. This region of high time-mean pressure is caused by the interaction between vane trailing edge and moving blades. The detailed unsteady flow physics in this region will be considered in more detail in Part II of this work. In the over-tip region (gauge rows 3–8) the circumferential differences in the static pressure become less defined, as the influence of the vane exit flow features reduces.

5. Conclusions

The spatial distributions of over-tip casing heat transfer rate, adiabatic wall temperature and Nusselt number have been successfully measured in the Oxford University transonic axial turbine test facility. The measurements have been obtained at flow conditions that are representative of those found in modern gas turbine engines. Both the heat transfer rate to the casing wall and the adiabatic wall temperature have been found to vary strongly with axial position through the turbine rotor. In contrast, the Nusselt number falls more gradually, dropping by 36% between rotor inlet and 80% axial chord. Indeed, the large variations in the measured heat transfer rate are primarily associated with changes in flow recovery temperature rather than changes in heat transfer coefficient. The influence of the nozzle guide vane exit flow features has been found to be small, although a region of higher heat transfer and higher static pressure has been seen in the vicinity of the vane trailing edges. The time-mean static pressure distribution on the over-tip casing wall has been measured and found to agree with expectations based on the blade loading distribution. These measurements also establish that circumferential variations in time-mean static pressure are small compared to the large reduction in static pressure that occurs across the blade row.

Acknowledgements

The support of Rolls-Royce plc and the Department of Trade and Industry is gratefully acknowledged. The authors would also like to acknowledge the generous support provided to Shin Yoshino by the Tokyo Electric Power Company (TEPCO). In addition, the experimental programme would not have been possible without the technical expertise of Mr. K.J. Grindrod and Mr. N.J. Brett.

Appendix A. Measurement uncertainty

The following discussion describes the estimated uncertainty in the heat transfer and pressure measurements. This is quoted as the 95% confidence limit, and follows the procedures outlined by Coleman and Steele (1995).

A.1. Heat transfer rate measurement uncertainty

Transient or short duration wind tunnels have been employed in heat transfer studies for many years and the sources of measurement uncertainty well documented (for example, Schultz and Jones, 1973). Following the

work of Coleman and Steele (1995) the uncertainty can be attributed to bias and precision limits in the fundamental measurement parameters. When measuring a steady heat transfer rate, the following equation describes the relationship between the surface temperature and the heat flux.

$$\dot{Q} = \frac{\mathrm{d}T_w}{\mathrm{d}\sqrt{t}} \frac{\sqrt{\pi}}{2} \sqrt{\rho c k} = \frac{\sqrt{\rho c k}}{\frac{\mathrm{d}R}{\mathrm{d}T_w} i_g} \frac{\sqrt{\pi}}{2} \frac{\mathrm{d}V_g}{\mathrm{d}\sqrt{t}}$$

The wall temperature, T_w is deduced from the gauge resistance, which is influenced by the uncertainties in the calibration of the heat transfer gauge and in the gauge current employed in the particular test. Therefore the overall measurement accuracy is dependent upon three fundamental sources of uncertainty: (1) the resistance versus temperature calibration for the gauge, $\mathrm{d}R/\mathrm{d}T_w$; (2) the gauge current, i_g; (3) the thermal product of the substrate material. Note that the measurement of gauge voltage, V_g is considered to involve comparatively small error compared to other sources of uncertainty since the analogue to digital converters are calibrated independently.

A.2. Uncertainty in heat transfer gauge calibration

The resistance of all heat transfer gauges was calibrated as a function of temperature in the range 20–60 °C using a temperature controlled water bath. An industrial standard Pt-100 platinum resistance probe was used as the primary temperature reference for the calibration of thin-film gauge resistance. Before calibration, a strict quality control check was placed on all heat transfer gauges in order to make sure that their responses displayed minimal levels of hysteresis. This criteria required a rigorous regime of annealing and temperature cycling of the instrumented Macor block. The uncertainty in the temperature coefficient, $\mathrm{d}R/\mathrm{d}T_w$ is estimated to be ±0.5%.

A.3. Uncertainty in gauge current

The heat transfer gauges were excited with a nominal constant current, i_g of 10 mA for all heat transfer measurements. The value of this constant current was measured for each gauge immediately prior to a test in the Rotor Facility. The uncertainty in gauge current is less than ±0.25%.

A.4. Uncertainty in substrate thermal product

When measuring heat transfer rates with thin-film gauges, the largest source of uncertainty is widely acknowledged to be the thermal product of the substrate. This parameter has been measured in previous studies for Macor machineable glass ceramic, with values ranging from 1765 (Miller, 1981) to 2090 (Arts and Derouvroit, 1992). For the purposes of the current work, the properties of the particular batch of ceramic were measured and a value of 1950 ± 4% employed in all the data analysis.

A.5. Overall uncertainty in the measured heat transfer rate

The above uncertainties can be considered as bias limits associated with the instrumentation. In addition, variations in the experimental run conditions lead to a precision limit that is estimated to be 4% based on run-to-run variations in Reynolds number. Combining the bias and precision limits, the overall uncertainty in heat flux is estimated to be 6%.

A.6. Adiabatic wall temperature measurement uncertainty

The measurement of adiabatic wall temperature is based upon interrogation of data such as those presented in Fig. 6. The uncertainty is influenced by a number of factors: (1) the number of measurement points used to define the straight line fit; (2) the temperature range achieved in the measurements; (3) the uncertainty in the heat flux measurement. A statistical analysis of the measurement data indicates that the measurement uncertainty is largest for the upstream gauges and reduces with increasing axial position. For example, in gauge row 1 the uncertainty is 4 K at 95% confidence, while at gauge row 8 it is 1.2 K at 95% confidence.

A.7. Nusselt number measurement uncertainty

The Nusselt number is defined according to Eq. (2). The measurement of Nusselt number is affected by uncertainties in the measured heat transfer rate and driver temperature. The previous discussions have established the uncertainty in heat transfer rate and adiabatic wall temperature measurements. The measurement uncertainty in time-mean Nusselt number is estimated to be 12% at 95% confidence.

A.8. Pressure measurement uncertainty

The measurement uncertainty associated with semiconductor pressure sensors is described in detail by Ainsworth et al. (2000). The Kulite pressure transducers used in this study were calibrated in the range 0.2–3.5 bar absolute using a digital pressure reference/controller. Additionally, the influence of temperature on the pressure sensor performance was calibrated in the temperature range 5–40 °C. The overall pressure measurement uncertainty is ±0.2% of full scale.

References

Ainsworth, R.W., Schultz, D.L., Davies, M.R.D., Forth, C.J.P., Hilditch, M.A., Oldfield, M.L.G., Sheard, A.G., 1988. A transient flow facility for the study of the thermofluid-dynamics of a full stage turbine under engine representative conditions. American Society of Mechanical Engineers, paper number 88-GT-144.

Ainsworth, R.W., Allen, J.L., Davies, M.R.D., Doorly, J.E., Forth, C.J.P., Hilditch, M.A., Oldfield, M.L.G., Sheard, A.G., 1989. Developments in instrumentation and processing for transient heat transfer measurement in a full-stage model turbine. Transactions of the American Society of Mechanical Engineers, Journal of Turbomachinery 111, 20–27.

Ainsworth, R.W., Miller, R.J., Moss, R.W., Thorpe, S.J., 2000. Unsteady pressure measurement. Measurement Science and Technology 11, 1055–1076.

Arts, T., Derouvroit, M.L., 1992. Aero-thermal performance of a 2-dimensional highly loaded transonic turbine nozzle guide vane—a test case for inviscid and viscous-flow computations. Transactions of the American Society of Mechanical Engineers, Journal of Turbomachinery 114 (1), 147–154.

Bindon, J.P., 1988. The measurement and formation of tip clearance loss. American Society of Mechanical Engineers, paper number 88-GT-203.

Bunker, R.S., 2001. A review of turbine blade tip heat transfer. Annals of the New York Academy of Sciences 934, 64–79.

Coleman, H.W., Steele, W.G., 1995. Engineering application of experimental uncertainty analysis. AIAA Journal 33 (10), 1888–1896.

Dailey, G., 2000. Aero-thermal performance of internal cooling systems in turbomachines. von Karman Institute Lecture Series 2000-03, The von Karman Institute, Brussels, Belgium.

Dietz, A.J., Ainsworth, R.W., 1992. Unsteady pressure measurements on the rotor of a model turbine stage in a transient flow facility. American Society of Mechanical Engineers, paper number 92-GT-156.

Garside, T., Moss, R.W., Ainsworth, R.W., Dancer, S.N., Rose, M.G., 1994. Heat transfer to rotating turbine blades in a flow undisturbed by wakes. American Society of Mechanical Engineers, paper number 94-GT-94.

Guenette, G.R., Epstein, A.H., Norton, R.J.G., Yuzhang, C., 1985. Time resolved measurements of a turbine rotor stationary tip casing pressure and heat transfer field. AIAA paper number 85-1220.

Heyes, F.J.G., Hodson, H.P., Dailey, G.M., 1992. The effect of blade tip geometry on the tip leakage flow in axial turbine cascades. Transactions of the American Society of Mechanical Engineers, Journal of Turbomachinery 114 (3), 643–651.

Kaiser, I., Bindon, J.P., 1997. The effect of tip clearance on the development of loss behind a rotor and a subsequent nozzle. American Society of Mechanical Engineers, paper number 97-GT-53.

Kim, Y.W., Metzger, D.E., 1995. Heat transfer and effectiveness on film cooled turbine blade tip models. Transactions of the American Society of Mechanical Engineers, Journal of Turbomachinery 117 (1), 12–21.

Kingcombe, R.C., Smith, I.M., Steeden, R.V., 1990. Over-tip pressure measurements in a cold-flow turbine rig. American Society of Mechanical Engineers, paper number 90-GT-312.

Meetham, G.W., 1984. Use of protective coatings in aero gas turbine engines. Materials Science and Technology 2 (3), 290–294.

Metzger, D.E., Dunn, M.G., Hah, C., 1991. Turbine tip and shroud heat transfer. Transactions of the American Society of Mechanical Engineers, Journal of Turbomachinery 113, 502–507.

Miller, C.G., 1981. Comparison of thin-film resistance heat-transfer gauges with the thin-skin transient calorimeter gauges in conventional hypersonic wind tunnels. NASA Technical Memorandum 83197.

Miller, R.J., Moss, R.W., Ainsworth, R.W., Harvey, N.W., 2003. Wake, shock and potential field interactions in a 1.5 stage turbine: part I—vane–rotor and rotor–vane interaction. Transactions of the American Society of Mechanical Engineers, Journal of Turbomachinery 125 (1), 33–39.

Moore, J., Moore, J.G., Henry, G.S., Chaudhry, U., 1988. Flow and heat transfer in turbine tip gaps. American Society of Mechanical Engineers, paper number 88-GT-188.

Papa, M., Goldstein, R.J., Gori, F., 2003. Effects of tip geometry and tip clearance on the mass/heat transfer from a large-scale gas turbine blade. Transactions of the American Society of Mechanical Engineers, Journal of Turbomachinery 125, 90–96.

Schlichting, H., Gersten, K., 2000. Boundary Layer Theory, 8th ed. Springer-Verlag, Berlin. pp. 645–646.

Schultz, D., Jones, T.V., 1973. Heat-transfer measurements in short-duration hypersonic facilities. AGARDograph No. 165, North Atlantic Treaty Organisation.

Spencer, M.C., Jones, T.V., Lock, G.D., 1996. Endwall heat transfer measurements in an annular cascade of nozzle guide vanes at engine representative Reynolds and Mach numbers. International Journal of Heat Fluid Flow 17, 139–147.

Srinivasan, V., Goldstein, R.J., 2003. Effect of endwall motion on blade tip heat transfer. Transactions of the American Society of Mechanical Engineers, Journal of Turbomachinery 125, 267–273.

Thorpe, S.J., Yoshino, S., Ainsworth, R.W., 2000. Fabrication and calibration techniques for turbine rotor tip heat transfer gauges. In: Symposium on Measuring Techniques in Transonic and Supersonic Flows in Cascades and Turbomachines, Florence, Italy.

Thorpe, S.J., Yoshino, S., Ainsworth, R.W., Harvey, N.W., 2004. An investigation of the heat transfer and static pressure field on the over-tip casing of a shroudless transonic turbine rotor at engine representative flow conditions. (II). Time-resolved results. International Journal of Heat and Fluid Flow vol. 25, doi:10.1016/j.ijheatfluidflow.2004.02.028.

Yamamoto, A., 1988. Endwall flow/loss mechanisms in a linear turbine cascade with blade tip-clearance. American Society of Mechanical Engineers, paper number 88-GT-235.